Alexandria Engineering Journal (2022) 61, 1938–1945

Alexandria University

Alexandria Engineering Journal

www.elsevier.com/locate/aej
www.sciencedirect.com

Magnetohydrodynamics (MHD) boundary layer flow of hybrid nanofluid over a moving plate with Joule heating

Najiyah Safwa Khashi'ie [a], **Norihan Md Arifin** [b,c], **Ioan Pop** [d,*]

[a] *Fakulti Teknologi Kejuruteraan Mekanikal dan Pembuatan, Universiti Teknikal Malaysia Melaka, Hang Tuah Jaya, 76100 Durian Tunggal, Melaka, Malaysia*
[b] *Institute for Mathematical Research, Universiti Putra Malaysia, 43400 UPM Serdang, Selangor, Malaysia*
[c] *Department of Mathematics, Faculty of Science, Universiti Putra Malaysia, 43400 UPM Serdang, Selangor, Malaysia*
[d] *Department of Mathematics, Babeş-Bolyai University, R-400084 Cluj-Napoca, Romania*

Received 14 May 2021; revised 27 June 2021; accepted 18 July 2021
Available online 13 August 2021

KEYWORDS

Hybrid nanofluid;
Heat transfer;
Joule heating;
Magnetohydrodynamics;
Moving plate;
Stability Analysis

Abstract The proficiency of hybrid nanoparticles in augmenting the heat transfer has fascinated many researchers to further analysing the working fluid. The present paper is focused on the MHD hybrid nanofluid flow with heat transfer on a moving plate with Joule heating. The combination of metal (Cu) and metal oxide (Al_2O_3) nanoparticles with water (H_2O) as the base fluid is used for the analysis. Similarity transformation reduces the complexity of the PDEs into a system of ODEs, which is then solved numerically using the function bvp4c from MATLAB for different values of the governing parameters. Two solutions are obtained when the plate is moved oppositely from the free stream flow. Analysis of flow stability unveils the first solution as the real physical solution, which is realizable in practice. From physical perspective, the real solution must be available for all cases of λ which affirms the finding from stability analysis. An upsurge of suction's strength and magnetic parameter enhances the heat transfer operation and extends the critical value λ_c. Meanwhile, there is no change on the critical value when the Eckert number is added. This study is important in determining the thermal behavior of Cu-Al_2O_3/H_2O when the physical parameters like magnetic field and Joule heating are embedded. The results are new and original with many practical applications in the modern industry.

1. Introduction

Hybrid nanofluids are widely used in the experimental and numerical investigations of fluid dynamics due to its significance in the thermal and energy performances. The available hybrid nanoparticles are usually formed from two types of

* Corresponding author.
E-mail address: popm.ioan@yahoo.co.uk (I. Pop).
Peer review under responsibility of Faculty of Engineering, Alexandria University.

https://doi.org/10.1016/j.aej.2021.07.032

nanoparticles like metal oxides (i.e., Fe_2O_3/hematite, Fe_3O_4/-magnetite, Al_2O_3/alumina, CuO/cupric oxide), carbon materials (i.e., CNT/carbon nanotube, graphite, MWCNT/multi-walled carbon nanotubes), metals (i.e., Ag/silver, Cu/copper) or metal carbide. The advantages of the Cu-Al_2O_3 hybrid nanoparticle were discussed by Suresh et al. [1,2] and led to the proposal of thermophysical properties' correlations for hybrid nanofluids by Devi and Devi [3] in analyzing a boundary layer flow problem. Takabi and Salehi [4] also proposed hybrid nanofluids' correlations which widely used in the numerical simulation of fluid motion. Huminic and Huminic [5] stated in their review paper that the hybrid nanofluids increased the thermal conductivity which led to the heat transfer enhancement in heat exchangers. Based on their experimental and numerical results, they indicated that the hybrid nanofluids could significantly improve the heat transfer in heat exchangers, but there were still a necessary research concerning to the study of different combinations of hybrid nanoparticles, mixing ratio, the hybrid nanofluids' stability, and the understanding of the mechanisms which contribute to the heat transfer augmentation. The exploration of numerical solutions in hybrid nanofluid flow was examined for different physical parameters and surfaces like movable plate [6–13], cylinder [14–18], disk [19–24] and thin needle [25–29].

Joule heating theoretically refers to the conversion of electric to thermal state energy which resulting in the development of heat from the resistive losses. This process is widely applied in the arrangement of electrical and electronic devices. From the viewpoint of boundary layer flow, this control parameter is used to increase the nanofluid's temperature as studied by Reddy and Reddy [30]. The effect of Joule heating in Cu-Al_2O_3/water along a stretching and shrinking cylinder was analyzed by Maskeen et al [31] and Khashi'ie et al. [32], respectively. Khashi'ie et al. [32] disclosed that the dimensionless Eckert number (from the Joule heating), has no impact in extending the point of separation which also in accordance with Yan et al. [33]. The perusal of MHD hybrid nanofluid flow with Joule heating and thermal radiation between two parallel plates was conducted by Chamkha et al. [34]. The impact of Joule heating on the nanofluid flow through a permeable duct has been analyzed by Li et al. [35]. Meanwhile, Saranya et al. [36] observed the viscous dissipation and Joule heating effects on the hybrid ferrofluid flow over a contracting cylinder. In their study, the magnetite-cobalt ferrite hybrid nanoparticles are used with the combination of water (50%) and ethylene glycol (50%) base fluid. Al-Mdallal et al. [37] investigated the simultaneous effect of inclined magnetic field and radiation parameter on the Marangoni hybrid nanofluid flow. The following interesting papers related to the energy transportation of nanofluids were also discussed by Renuka et al. [38], Soomro et al. [39], Ul Haq [40], Al-Mdallal et al. [41], Ziyad et al. [42] and Wahid et al. [43].

This work studies the hybrid nanofluid from Cu-Al_2O_3/water formation with Joule heating and magnetic field. The single-phase model of Cu-Al_2O_3/water is formulated and transformed into a reduced differential equations via the similarity transformation. The bvp4c application is used for the results' generation and validated based on the available numerical values from the previous works. We are confident with the novelty of the theoretical findings from this work.

2. Physical model

Let us consider the boundary layer flow of a hybrid Cu-Al_2O_3/H_2O nanofluid past a permeable flat plate as it is shown in Fig. 1, where the x and y axes are the Cartesian coordinates with the $x-$ axis measured along the plate and y - axis is normal to it, the flow being in the region $y \geq 0$. The free stream of Cu-Al_2O_3/H_2O has a fixed velocity U. The plate is moving with the velocity $U\lambda$, where λ corresponds to the moving plate, away from the origin ($\lambda > 0$)and to the origin ($\lambda < 0$), respectively. It is assumed that the mass fluid velocity is v_w with $v_w < 0$ for suction and $v_w > 0$ for injection, respectively. Aly et al. [44] reported that similarity solutions are possible if the magnetic field has the special form of $B = B_0 x^{-1/2}$. Furthermore, the small magnetic Reynolds number from induced magnetic field is ignored. The moving plate temperature is T_w, while the temperature of the far field is T_∞.

Under these assumptions, the governing boundary layer equations of the mass, momentum and energy hybrid nanofluids can be written as (Devi and Devi [3]):

$$\frac{\partial u}{\partial x} + \frac{\partial v}{\partial y} = 0, \tag{1}$$

$$u\frac{\partial u}{\partial x} + v\frac{\partial u}{\partial y} = \frac{\mu_{hnf}}{\rho_{hnf}}\frac{\partial^2 u}{\partial y^2} - \frac{\sigma_{hnf}}{\rho_{hnf}}B^2(u-U), \tag{2}$$

$$u\frac{\partial T}{\partial x} + v\frac{\partial T}{\partial y} = \frac{k_{hnf}}{(\rho C_p)_{hnf}}\frac{\partial^2 T}{\partial y^2} + \frac{\sigma_{hnf}}{(\rho C_p)_{hnf}}B^2(u-U)^2, \tag{3}$$

The associate boundary conditions are

$$\begin{aligned} &u = \lambda U, v = v_w, T = T_w at y = 0 \\ &u \to U, T = T_\infty as y \to \infty \end{aligned} \tag{4}$$

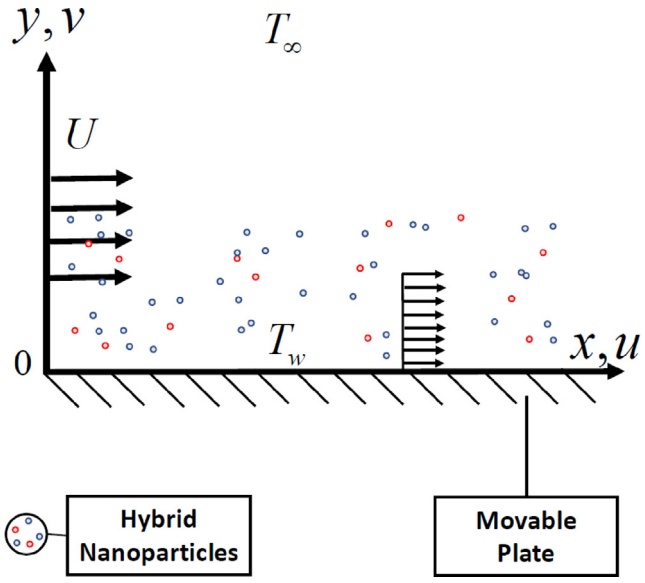

Fig. 1 Physical illustration with coordinate system.

Table 1 Hybrid nanofluid's correlations (Takabi and Salehi [4]).

Properties	Hybrid Nanofluid
Density (ρ)	$\rho_{hnf} = (1-\phi_{hnf})\rho_f + \phi_1\rho_{s1} + \phi_2\rho_{s2}$
Heat Capacity (ρC_p)	$(\rho C_p)_{hnf} = (1-\phi_{hnf})(\rho C_p)_f + \phi_1(\rho C_p)_{s1} + \phi_2(\rho C_p)_{s2}$
Dynamic Viscocity (μ)	$\frac{\mu_{hnf}}{\mu_f} = \frac{1}{(1-\phi_{hnf})^{2.5}}$
Thermal Conductivity (k)	$\frac{k_{hnf}}{k_f} = \left[\frac{\left(\frac{\phi_1 k_1+\phi_2 k_2}{\phi_{hnf}}\right) + 2k_f + 2(\phi_1 k_1+\phi_2 k_2) - 2\phi_{hnf}k_f}{\left(\frac{\phi_1 k_1+\phi_2 k_2}{\phi_{hnf}}\right) + 2k_f - (\phi_1 k_1+\phi_2 k_2) + \phi_{hnf}k_f}\right]$
Electrical Conductivity (k)	$\frac{\sigma_{hnf}}{\sigma_f} = \left[\frac{\left(\frac{\phi_1 \sigma_1+\phi_2 \sigma_2}{\phi_{hnf}}\right) + 2\sigma_f + 2(\phi_1 \sigma_1+\phi_2 \sigma_2) - 2\phi_{hnf}\sigma_f}{\left(\frac{\phi_1 \sigma_1+\phi_2 \sigma_2}{\phi_{hnf}}\right) + 2\sigma_f - (\phi_1 \sigma_1+\phi_2 \sigma_2) + \phi_{hnf}\sigma_f}\right]$

Table 2 Thermophysical properties for pure water and nanoparticles (Oztop and Abu-Nada [45].

Thermophysical Properties	H_2O	Nanoparticles	
		Al_2O_3	Cu
$\rho(\mathrm{kg}m^{-3})$	997.1	3970	8933
$C_p(Jkg^{-1}K^{-1})$	4179	765	385
$k(\mathrm{W}m^{-1}K^{-1})$	0.6130	40	400

For the evaluation of the thermophysical properties in Table 1, the correlations by Takabi and Salehi [4] are adopted which are feasible and built based on the physical assumptions where $\phi_{hnf} = \phi_1 + \phi_2$. Meanwhile, Table 2 display the the physical properties of the pure water and nanoparticles.

Now, the following similarity variables are introduced (Weidman et al. [46])

$$\left.\begin{aligned} u = Uf'(\eta), v = \sqrt{\tfrac{Uv_f}{2x}}\left[\eta f'(\eta) - f(\eta)\right], \eta = y\sqrt{\tfrac{U}{2xv_f}} \\ \psi = \sqrt{2v_f x U} f(\eta), \theta(\eta) = \tfrac{T-T_\infty}{T_w-T_\infty} \end{aligned}\right\} \tag{5}$$

while the transpiration effect through the permeable plates is defined as

$$v_w = -\sqrt{\frac{Uv_f}{2x}}S, \tag{6}$$

where S is the mass flux velocity with $S > 0$ for suction and $S < 0$ for fluid injection. Substituting (6) in Eqs. (2) and (3), the transformed ODEs and boundary conditions are

$$\left(\frac{\mu_{hnf}/\mu_f}{\rho_{hnf}/\rho_f}\right)f''' + ff'' - \left(\frac{\sigma_{hnf}/\sigma_f}{\rho_{hnf}/\rho_f}\right)M(f'-1) = 0, \tag{7}$$

$$\frac{1}{\mathrm{Pr}}\frac{k_{hnf}/k_f}{(\rho C_p)_{hnf}/(\rho C_p)_f}\theta'' + f\theta' + \left(\frac{\sigma_{hnf}/\sigma_f}{(\rho C_p)_{hnf}/(\rho C_p)_f}\right)EcM(f'-1)^2 = 0, \tag{8}$$

$$\left.\begin{aligned} f(0) = S, f'(0) = \lambda, \theta(0) = 1 \\ f'(\eta) \to 1, \theta(\eta) \to 0 as \eta \to \infty \end{aligned}\right\} \tag{9}$$

where Pr is the Prandtl number, M is the magnetic parameter and Ec is the Eckert number, which are defined as

$$\mathrm{Pr} = \frac{(\mu C_p)_f}{k_f},\ M = \frac{2\sigma_f B_0^2}{U\rho_f},\ Ec = \frac{U^2}{(C_p)_f(T_w - T_\infty)}, \tag{10}$$

The physical quantities of interest are the skin friction coefficient C_f and the local Nusselt number Nu_x, which are defined as

$$C_f = \frac{\mu_{hnf}}{\rho_f U^2}\left(\frac{\partial u}{\partial y}\right)_{y=0}, \quad Nu_x = -\frac{xk_{hnf}}{k_f(T_w - T_\infty)}\left(\frac{\partial T}{\partial y}\right)_{y=0} \tag{11}$$

Applying (5) into (11), we get the reduced form of skin friction coefficient and heat transfer rate such that

$$\sqrt{2}Re_x^{1/2}C_f = \frac{\mu_{hnf}}{\mu_f}f''(0)\ , \quad \sqrt{2}Re_x^{-1/2}Nu_x = -\frac{k_{hnf}}{k_f}\theta'(0) \tag{12}$$

where $Re_x = Ux/v_f$ is the local Reynolds number.

3. Flow stability

Merkin [47] contributed to the discovery of stability analysis by considering an unsteady case. Using this analysis, the real physical solution is evolved with time accompanying the small-

est error. The detail procedures of flow stability for a basic moving plate case were discussed by Zainal et al. [6], Aladdin et al. [9] and Khashi'ie et al. [11]. By inserting Eqs. (2) and (3) with the unsteady term, the equations are

$$\frac{\partial u}{\partial t}+u\frac{\partial u}{\partial x}+v\frac{\partial u}{\partial y}=\frac{\mu_{hnf}}{\rho_{hnf}}\frac{\partial^2 u}{\partial y^2}+\frac{\sigma_{hnf}}{\rho_{hnf}}B^2(U-u) \tag{13}$$

$$\frac{\partial T}{\partial t}+u\frac{\partial T}{\partial x}+v\frac{\partial T}{\partial y}=\frac{k_{hnf}}{(\rho C_p)_{hnf}}\frac{\partial^2 T}{\partial y^2}+\frac{\sigma_{hnf}}{(\rho C_p)_{hnf}}B^2(u-U)^2. \tag{14}$$

with new similarity transformation

$$\left.\begin{aligned} u=\tfrac{\partial\psi}{\partial y}, v=-\tfrac{\partial\psi}{\partial x}, \psi=\sqrt{2Uv_x x}f(\eta,\tau), \eta=y\sqrt{\tfrac{U}{2v_f x}}\\ \theta(\eta,\tau)=\tfrac{T-T_\infty}{T_w-T_\infty}, \tau=\tfrac{U}{2x}t \end{aligned}\right\} \tag{15}$$

Referring to Zainal et al. [6], Aladdin et al. [9] and Khashi'ie et al. [11],

$$\begin{aligned} u&=\tfrac{\partial\psi}{\partial y}=\tfrac{\partial\psi}{\partial f}\tfrac{\partial f}{\partial\eta}=U\tfrac{\partial f}{\partial\eta},\\ v&=-\tfrac{\partial\psi}{\partial x}=\left(\tfrac{Uv_f}{2x}\right)^{1/2}\left[\eta\tfrac{\partial f}{\partial\eta}+2\tau\tfrac{\partial f}{\partial\tau}-f\right] \end{aligned} \tag{16}$$

so that

$$\begin{aligned} &\left(\frac{\mu_{hnf}/\mu_f}{\rho_{hnf}/\rho_f}\right)\frac{\partial^3 f}{\partial\eta^3}+f\frac{\partial^2 f}{\partial\eta^2}-\left(\frac{\sigma_{hnf}/\sigma_f}{\rho_{hnf}/\rho_f}\right)M\left(\frac{\partial f}{\partial\eta}-1\right)\\ &+2\tau\left(\frac{\partial f}{\partial\eta}\frac{\partial^2 f}{\partial\eta\partial\tau}-\frac{\partial f}{\partial\tau}\frac{\partial^2 f}{\partial\eta^2}\right)-\frac{\partial^2 f}{\partial\eta\partial\tau}\\ &=0, \end{aligned} \tag{17}$$

$$\begin{aligned} &\tfrac{1}{\Pr}\frac{k_{hnf}/k_f}{(\rho C_p)_{hnf}/(\rho C_p)_f}\frac{\partial^2\theta}{\partial\eta^2}+f\frac{\partial\theta}{\partial\eta}+\left(\frac{\sigma_{hnf}/\sigma_f}{(\rho C_p)_{hnf}/(\rho C_p)_f}\right)EcM\left(\frac{\partial f}{\partial\eta}-1\right)^2\\ &+2\tau\left(\tfrac{\partial f}{\partial\eta}\tfrac{\partial\theta}{\partial\tau}-\tfrac{\partial f}{\partial\tau}\tfrac{\partial\theta}{\partial\eta}\right)-\tfrac{\partial\theta}{\partial\tau}=0, \end{aligned} \tag{18}$$

$$\begin{aligned} &\tfrac{\partial f}{\partial\eta}(0,\tau)=\lambda,\ f(0,\tau)=S,\ \theta(0,\tau)=1,\\ &\tfrac{\partial f}{\partial\eta}(\infty,\tau)\to 1,\ \theta(\infty,\tau)\to 0. \end{aligned} \tag{19}$$

Next procedure is to allow the disturbance in Eqs. (17)–(19) by adopting the perturbation method (Weidman et al. [46])

$$\left.\begin{aligned} f(\eta,\tau)&=f_0(\eta)+e^{-\gamma\tau}F(\eta,\tau)\\ \theta(\eta,\tau)&=\theta_0(\eta)+e^{-\gamma\tau}G(\eta,\tau) \end{aligned}\right\}, \tag{20}$$

where $f=f_0(\eta)$, $\theta=\theta_0(\eta)$ while $F(\eta)$ and $G(\eta)$ are functions which related to f_0 and θ_0, respectively. The eigenvalue γ is used to measure the stability of solutions. The solutions' stability is dependable on the smallest eigenvalue γ_1 where positive value indicates the real physical solution. In this study, we investigate the stability of the similarity solution $f_0(\eta)$ and $\theta_0(\eta)$ by setting $\tau=0$, and hence identify the initial growth or decay of the solution (20). To test our numerical procedure, we need to solve the linear eigenvalue problem.

The simplified linearized eigenvalue equations and conditions are

$$\frac{\mu_{hnf}/\mu_f}{\rho_{hnf}/\rho_f}F'''+f_0F''+Ff_0''+\gamma F'-\left(\frac{\sigma_{hnf}/\sigma_f}{\rho_{hnf}/\rho_f}\right)M(F'-1)=0, \tag{21}$$

$$\begin{aligned} &\frac{1}{\Pr}\frac{k_{hnf}/k_f}{(\rho C_p)_{hnf}/(\rho C_p)_f}G''+F\theta_0'+f_0G'+\gamma G\\ &+\left(\frac{\sigma_{hnf}/\sigma_f}{(\rho C_p)_{hnf}/(\rho C_p)_f}\right)EcM(F'-1)^2=0, \end{aligned} \tag{22}$$

$$F(0)=0,\ F'(0)=0,\ G(0)=0,\ F'(\infty)\to 0,\ G(\infty)\to 0. \tag{23}$$

To avoid zero eigenvalues, it is suggested to relax any suitable conditions at $\eta\to\infty$ and replace with a condition at $\eta=0$ (Harris et al. [48]). Hence, the relaxing condition of (23) is given by

$$F(0)=0,\ F'(0)=0,\ F''(0)=1,\ G(0)=0,\ G(\infty)\to 0. \tag{24}$$

4. Results and discussion

Similarity Eqs. (7)–(9) are dealt with the bvp4c solver procurable in the Matlab software. The numerical solutions are presented in both tables and figures. It is expected that two solutions exist with the consideration of various values of moving parameter: $\lambda>0$ denotes the same path between moving plate and free stream flow while $\lambda<0$ indicates the different orientation. Other parameters are $0\leqslant S\leqslant 0.5$, $0\leqslant M\leqslant 0.02$, $0\leqslant Ec\leqslant 1$ and $0\leqslant\phi_1,\phi_2\leqslant 0.01$ based on the solutions' location. Before generating the solutions, few of validation tests with previous similar findings are conducted to verify the accuracy of present model as showed in Tables 3 and 4. Since hybrid nanofluid and Joule heating being the main focus of this work, the comparisons are limited to the viscous working fluid and single nanofluid with the exclusion of the control parameter. A comparison is made for different values of S with those of Weidman et al. [46], when $\phi_1=\phi_2=0$ (regular fluid) and $M=0$ (the comparison is presented in Table 3). Both results are compatible and in very good agreement. Furthermore, for the exclusion of magnetic and suction/injection parameter, $\lambda_c=-0.3541$ is also visible and validated in Figs. 4 and 5. Meanwhile, Table 4 shows the available solutions of $f''(0)$ when $\phi_1=0,\phi_2=0.1$ and $M=S=0$ which are consistent with Zainal et al. [6] and Rohni et al. [49].

Table 5 display the smallest eigenvalue for selected values of λ in the measurement of solutions' stability. The first solution has positive eigenvalue which implies that solution's stability while negative eigenvalue (second solution) denotes the unstableness of the solution. Another observation from this analysis is both eigenvalues approaching to zero value as $\lambda\to\lambda_c$ which in accordance with Merkin [47].

Table 3 Validation test for the critical value λ_c with suction/injection parameter.

S	Present	Weidman et al. [46]
−0.50	−0.10388	−0.1035
−0.25	−0.21461	−0.2125
0.00	−0.35410	−0.3541
0.25	−0.52238	−0.5224
0.50	−0.72001	−0.7200

Table 4 First and second solutions of $f''(0)$ when $\phi_1 = 0$, $\phi_2 = 0.1$, and $M = S = 0$.

λ	Present		Zainal et al. [6]		Rohni et al. [49]	
	First	Second	First	Second	First	Second
−0.1000	0.541615	0.002274	0.541615	0.002274	0.5416	0.0023
−0.1500	0.527547	0.010169	0.527547	0.010169	0.5276	0.0102
−0.2000	0.505318	0.026061	0.505318	0.026061	0.5053	0.0261
−0.2500	0.471688	0.053322	0.471688	0.053322	0.4717	0.0533
−0.3000	0.418959	0.099702	0.418959	0.099702	0.4190	0.0997
−0.3500	0.302592	0.209761	0.302592	0.209761	0.3028	0.2098
−0.3541	0.257961	0.253877	0.257961	0.253877	0.2623	–

Table 5 Analysis of flow stability for the first and second solutions.

λ	$\gamma_{1,\text{First}}$	$\gamma_{1,\text{Second}}$
−0.369	0.01707	−0.02882
−0.3693	0.01227	−0.02465
−0.3697	0.00302	−0.01625
−0.36973	0.00197	−0.01526
−0.36975	0.00119	−0.01453

Figs. 2 and 3 highlight the distribution of $\sqrt{2}Re_x^{1/2}C_f$ and $\sqrt{2}Re_x^{-1/2}Nu_x$ towards dimensionless λ with suction effect $S = 0, 0.25, 0.5$. The appearance of two solutions is recognized, but the availability of second solution is confined within a specific range of λ as displayed in Figs. 2 and 3. At $\lambda = 1$, the skin friction is not produced ($f''(0) = 0$) because both plate and free stream hybrid nanofluid move with an equal velocity (Khashi'ie et al. [11]). It is worth to point out that $\lambda > 0$ indicates the same direction of the movement between the hybrid nanofluid and the plate while $\lambda < 0$refers to the opposite direction of the fluid motion and plate. As the suction strength enhances, both $\sqrt{2}Re_x^{1/2}C_f$ and $\sqrt{2}Re_x^{-1/2}Nu_x$ augment. However, for the distribution of skin friction coefficient, the flow

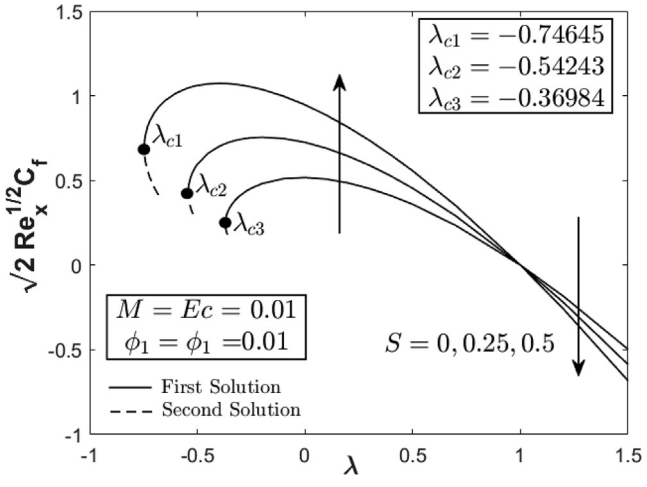

Fig. 2 Distribution of skin friction coefficient with various λ and S.

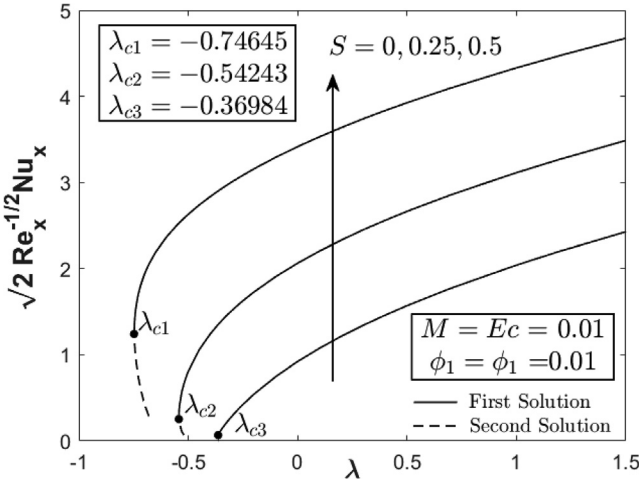

Fig. 3 Distribution of heat transfer coefficient with various λ and S.

characteristics change when $\lambda > 1$. The role of suction which induce the fluid motion simultaneously, assists the heated particles towards the wall which then, increases the heat transfer rate as depicted in Fig. 3. For each S, the heat transfer rate slightly augments when $\lambda \to +\lambda$ which means that the direction of the hybrid nanofluid and plate is one of the factor in enhancing the heat transfer performance of the working fluid.

Figs. 4 and 5 show the variations of $\sqrt{2}Re_x^{1/2}C_f$ and $\sqrt{2}Re_x^{-1/2}Nu_x$with ascending values of magnetic parameter. Both skin friction coefficient and heat transfer rate slightly increase with the accretion of magnetic parameter, but it is found that when $\lambda > 1$, both distributions start to deteriorate slightly. Another observation is the rising values of $M = 0, 0.01, 0.02$ extends the separation value (indicator of the boundary layer separation). From fundamental perspective, the magnetic field formed a drag/resistance Lorentz force which oppose the fluid motion, and consequently delay the separation of boundary layer. But, if the free stream velocity is less than the moving plate velocity ($\lambda < 1$), this condition helps in increasing and stabilizing the fluid velocity as the magnetic parameter imposed. However, if the moving plate velocity is dominant, the basic fundamental is applied where the velocity of this hybrid nanofluid deteriorates as clarified in Fig. 6 (velocity profile). Coincidently, the heat is actively produced from the generation of Lorentz force when $\lambda < 1$ which

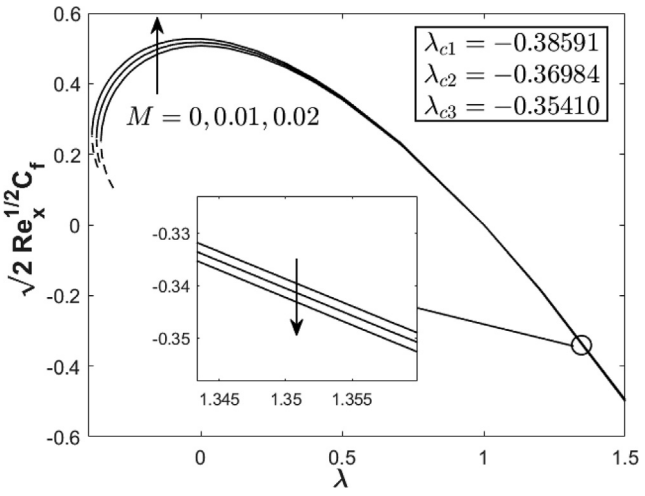

Fig. 4 Distribution of skin friction coefficient with various λ and M.

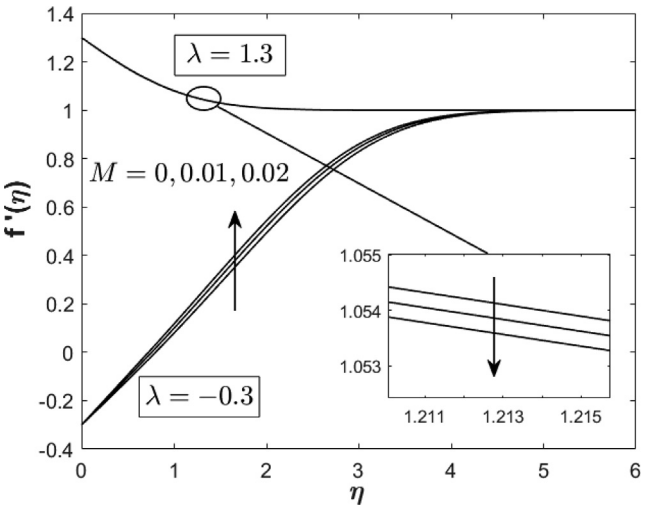

Fig. 6 Velocity profile with various λ and M when $S = 0, Ec = 0.01$ and $\phi_1 = \phi_2 = 0.01$.

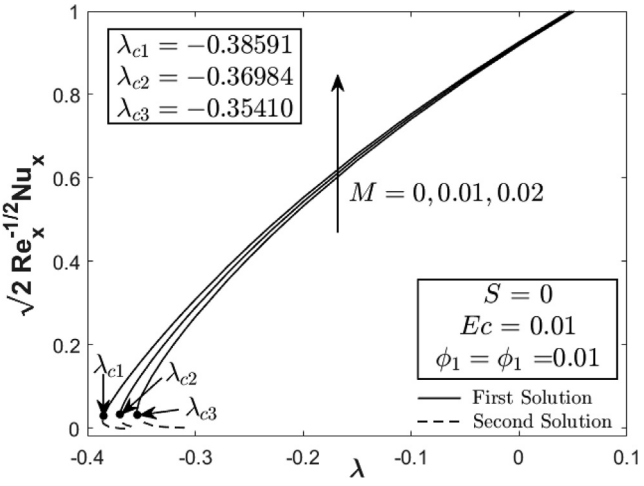

Fig. 5 Distribution of heat transfer coefficient with various λ and M.

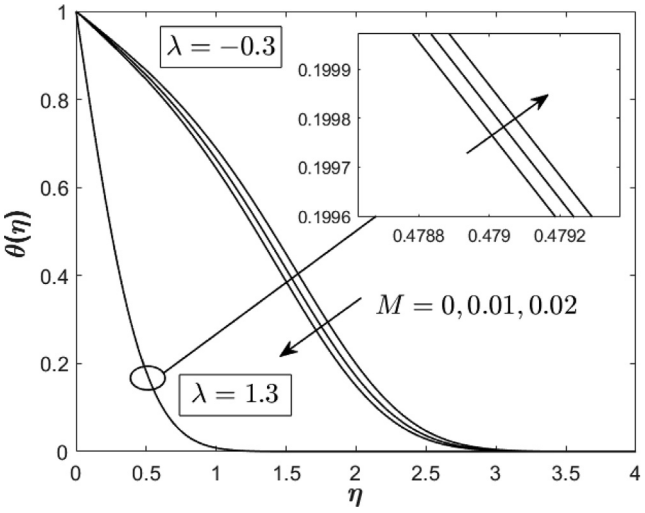

Fig. 7 Temperature profile with various λ and M when $S = 0, Ec = 0.01$ and $\phi_1 = \phi_2 = 0.01$.

increase the hybrid nanofluid temperature whilst circulate an active heat transfer process. However, opposite behavior is observed for $\lambda > 1$ as clarified in Figs. 5 and 7.

Further observation from Figs. 2 to 5, the dual solutions (upper and lower branch solutions) exist for $\lambda_c < \lambda < 0$ and no solutions exist for $\lambda < \lambda_c$, where $\lambda_c < 0$ is the critical value of $\lambda < 0$ for which Eqs. (7) and (8) subject to the boundary conditions (9) have no solution. However, for $\lambda < \lambda_c$, the full Navier–Stokes and energy equations have to be solved. Further, it is seen from the stability analysis that the upper branch solutions are stable and physically realizable, while the lower branch solutions are unstable and, therefore, not physically realizable.

Fig. 8 depicts the impact of Ec on the heat transfer distribution. This Eckert number arise from the implementation of the coupled effects of Joule heating and magnetic field. Joule heating (including magnetic field) produces heat from the electric current source to the conducting moving plate. The increment of Eckert number may inflate the temperature profile as portrayed in Fig. 9 whilst reduce the heat transfer distribution. However, the separation value remains at $\lambda_c = -0.36984$ for each $Ec = 0.01, 0.1, 1$ which implies that the rise of Eckert number is not affecting the fluid motion.

5. Conclusions

This novel work presents a numerical study of MHD hybrid Cu-Al_2O_3/water nanofluid flow on a movable plate with Joule heating effect. The physical phenomenon follows the usual approximations of boundary layer flow while the bvp4c programme is used for the generation of the results. Two solutions are observed which lead to the stability analysis where the first solution is validated as the real physical solution (physically realizable in practice). Dual solutions exist for the case $\lambda < 0$ which bifurcate at the critical value λ_c. An upsurge of suction's strength and magnetic parameter enhances the heat transfer operation and extends the critical value. As the magnetic

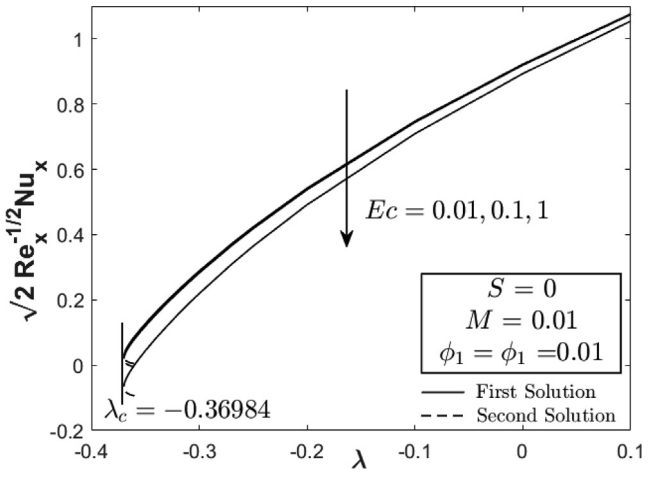

Fig. 8 Distribution of heat transfer coefficient with various λ and Ec.

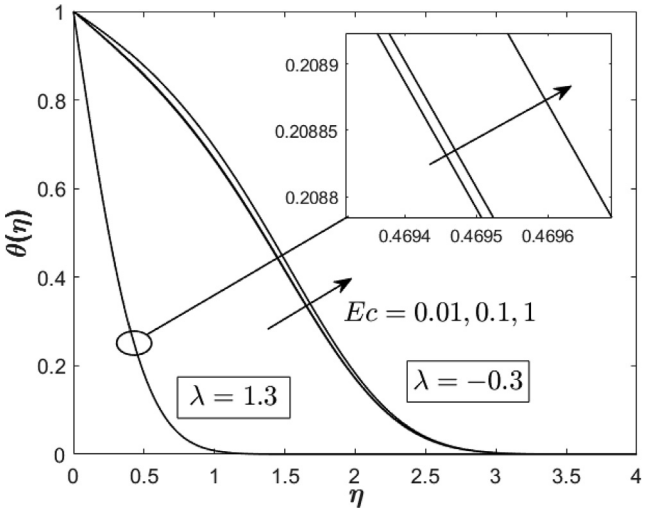

Fig. 9 Temperature profile with various λ and Ec when $S = 0, M = 0.01$ and $\phi_1 = \phi_2 = 0.01$.

parameter increases, the velocity and temperature profiles show disparate behavior when $\lambda < 0$ and $\lambda > 0$ are considered. Meanwhile, the Eckert number (arise from Joule heating) gives no influence on the boundary layer separation and reduces the heat transfer rate of the working fluid. From this study, it is recommended for the cooling/heating industries to enhance the heat transfer operation by inserting a small scale of suction and magnetic field effects.

Declaration of Competing Interest

The authors declare that they have no known competing financial interests or personal relationships that could have appeared to influence the work reported in this paper.

Acknowledgements

We acknowledge the financial support from Babeş-Bolyai University including the research support from Universiti Teknikal Malaysia Melaka and Universiti Putra Malaysia.

References

[1] S. Suresh, K.P. Venkitaraj, P. Selvakumar, M. Chandrasekar, Synthesis of Al_2O_3–Cu/water hybrid nanofluids using two step method and its thermo physical properties, Colloids Surf. A: Phys. Eng. Aspects 388 (1–3) (2011) 41–48.

[2] S. Suresh, K.P. Venkitaraj, P. Selvakumar, M. Chandrasekar, Effect of Al_2O_3–Cu/water hybrid nanofluid in heat transfer, Exp. Therm. Fluid Sci. 38 (2012) 54–60.

[3] S.P.A. Devi, S.S.U. Devi, Numerical investigation of hydromagnetic hybrid Cu–Al2O3/water nanofluid flow over a permeable stretching sheet with suction, Int. J. Nonlin. Sci. Numer. Simul. 17 (5) (2016) 249–257.

[4] B. Takabi, S. Salehi, Augmentation of the heat transfer performance of a sinusoidal corrugated enclosure by employing hybrid nanofluid, Adv. Mech. Eng. 6 (2014) 147059.

[5] G. Huminic, A. Huminic, Hybrid nanofluids for heat transfer applications – A state-of-the-art review, Int. J. Heat Mass Transf. 125 (2018) 82–103.

[6] N.A. Zainal, R. Nazar, K. Naganthran, I. Pop, MHD flow and heat transfer of hybrid nanofluid over a permeable moving surface in the presence of thermal radiation, Int. J. Numer Methods Heat Fluid Flow 31 (3) (2021) 858–879.

[7] N.A. Zainal, R. Nazar, K. Naganthran, I. Pop, Unsteady EMHD stagnation point flow over a stretching/shrinking sheet in a hybrid Al_2O_3-Cu/H2O nanofluid, Int. Comm. Heat Mass Transf. 123 (2021) 105205.

[8] N.S. Anuar, N. Bachok, I. Pop, Influence of buoyancy force on Ag-MgO/water hybrid nanofluid flow in an inclined permeable stretching/shrinking sheet, Int. Comm. Heat Mass Transf. 123 (2021) 105236.

[9] N.A. Aladdin, N. Bachok, I. Pop, Cu-Al_2O_3/water hybrid nanofluid flow over a permeable moving surface in presence of hydromagnetic and suction effects, Alexandria Eng. J. 59 (2) (2020) 657–666.

[10] N.A. Aladdin, N. Bachok, Boundary Layer Flow and Heat Transfer of Al_2O_3-TiO_2/Water Hybrid Nanofluid over a Permeable Moving Plate, Symmetry 12 (7) (2020) 1064.

[11] N.S. Khashi'ie, N.M. Arifin, I. Pop, R. Nazar, Melting heat transfer in hybrid nanofluid flow along a moving surface, J. Therm. Anal. Calorim. (2020). https://doi.org/10.1007/s10973-020-10238-4.

[12] S. Suganya, M. Muthtamilselvan, Z.A. Alhussain, Activation energy and Coriolis force on Cu-TiO2/water hybrid nanofluid flow in an existence of nonlinear radiation, Appl. Nanosci. 11 (2021) 933.

[13] S.A. Bakar, N.M. Arifin, N.S. Khashi'ie, N. Bachok, Hybrid Nanofluid Flow over a Permeable Shrinking Sheet Embedded in a Porous Medium with Radiation and Slip Impacts, Mathematics 9(8) (2021) 878

[14] N.S. Khashi'ie, I. Waini, N.A. Zainal, K. Hamzah, A.R.M. Kasim, Hybrid Nanofluid Flow Past a Shrinking Cylinder with Prescribed Surface Heat Flux, Symmetry 12(9) (2020) 1493

[15] I. Waini, A. Ishak, I. Pop, Hybrid nanofluid flow towards a stagnation point on a stretching/shrinking cylinder, Sci. Rep. 10 (1) (2020) 1–12.

[16] N.S. Khashi'ie, E.H. Hafidzuddin, N.M. Arifin, N. Wahi, Stagnation point flow of hybrid nanofluid over a permeable

vertical stretching/shrinking cylinder with thermal stratification effect, CFD Lett. 12(2) (2020) 80-94.
[17] E.M. Elsaid, M.S. Abdel-wahed, Impact of hybrid nanofluid coolant on the boundary layer behavior over a moving cylinder: Numerical case study, Case Studies Therm. Eng. 25 (2021) 100951.
[18] U. Rashid, H. Liang, H. Ahmad, M. Abbas, A. Iqbal, Y.S. Hamed, Study of (Ag and TiO_2)/water nanoparticles shape effect on heat transfer and hybrid nanofluid flow toward stretching shrinking horizontal cylinder, Results Phys. 21 (2021) 103812.
[19] U. Farooq, M.I. Afridi, M. Qasim, D.C. Lu, Transpiration and viscous dissipation effects on entropy generation in hybrid nanofluid flow over a nonlinear radially stretching disk, Entropy 20 (9) (2018) 668.
[20] N.C. Roşca, A.V. Roşca, I. Pop, Axisymmetric flow of hybrid nanofluid due to a permeable non-linearly stretching/shrinking sheet with radiation effect, Int. J. Numer. Methods Heat Fluid Flow (2020), https://doi.org/10.1108/HFF-09-2020-0574.
[21] N.S. Khashi'ie, N.M. Arifin, I. Pop, Unsteady axisymmetric flow and heat transfer of a hybrid nanofluid over a permeable stretching/shrinking disc, Int. J. Numer. Methods Heat Fluid Flow 31(6) (2021) 2005-2021.
[22] U. Khan, I. Waini, A. Ishak, I. Pop, Unsteady hybrid nanofluid flow over a radially permeable shrinking/stretching surface, J. Mol. Liq. 331 (2021) 115752.
[23] M. Shoaib, M.A. Raja, M.T. Sabir, M. Awais, S. Islam, Z. Shah, P. Kumam, Numerical analysis of 3-D MHD hybrid nanofluid over a rotational disk in presence of thermal radiation with Joule heating and viscous dissipation effects using Lobatto IIIA technique, Alexandria Eng. J. 60 (4) (2021) 3605–3619.
[24] N.S. Wahid, N.M. Arifin, N.S. Khashi'ie, I. Pop, Marangoni hybrid nanofluid flow over a permeable infinite disk embedded in a porous medium, Int. Comm. Heat Mass Transf. 126 (2021) 105421.
[25] N. Abbas, M.Y. Malik, S. Nadeem, I.M. Alarifi, On extended version of Yamada-Ota and Xue models of hybrid nanofluid on moving needle, Eur. Phys. J Plus 135 (2) (2020) 145.
[26] I. Waini, A. Ishak, I. Pop, Hybrid nanofluid flow past a permeable moving thin needle, Mathematics 8 (4) (2020) 612.
[27] I. Waini, A. Ishak, I. Pop, Hybrid nanofluid flow and heat transfer past a vertical thin needle with prescribed surface heat flux, Int. J. Numer. Methods Heat Fluid Flow 29 (12) (2020) 4875–4894.
[28] N.A. Aladdin, N. Bachok, I. Pop, Boundary layer flow and heat transfer of Cu-Al_2O_3/water over a moving horizontal slender needle in presence of hydromagnetic and slip effects, Int. Comm. Heat Mass Transf. 123 (2021) 105213.
[29] V. Puneeth, S. Manjunatha, O.D. Makinde, B.J. Gireesha, Bioconvection of a radiating hybrid nanofluid past a thin needle in the presence of heterogeneous–homogeneous chemical reaction, J. Heat Transf. 143 (4) (2021) 042502.
[30] M.G. Reddy, K.V. Reddy, Influence of Joule Heating on MHD Peristaltic Flow of a Nanofluid with Compliant Walls, Procedia Eng. 127 (2015) 1002–1009.
[31] M.M. Maskeen, A. Zeeshan, O.U. Mehmood, M. Hassan, Heat transfer enhancement in hydromagnetic alumina–copper/water hybrid nanofluid flow over a stretching cylinder, J. Therm. Anal. Calorim. 138 (2) (2019) 1127–1136.
[32] N.S. Khashi'ie, N.M. Arifin, I. Pop, N.S. Wahid, Flow and heat transfer of hybrid nanofluid over a permeable shrinking cylinder with Joule heating: a comparative analysis, Alexandria Eng. J. 59 (3) (2020) 1787–1798.
[33] L. Yan, S. Dero, I. Khan, I.A. Mari, D. Baleanu, K.S. Nisar, E. S. Sherif, H.S. Abdo, Dual Solutions and Stability Analysis of Magnetized Hybrid Nanofluid with Joule Heating and Multiple Slip Conditions, Processes 8 (3) (2020) 332.
[34] A.J. Chamkha, A.S. Dogonchi, D.D. Ganji, Magneto-hydrodynamic flow and heat transfer of a hybrid nanofluid in a rotating system among two surfaces in the presence of thermal radiation and Joule heating, AIP Adv. 9 (2) (2019) 025103.
[35] Li. Z., A. Shafee, R. Kandasamy, M. Ramzan, Q. Al-Mdallal, Nanoparticle transportation through a permeable duct with Joule heating influence. Microsystem Technologies: micro and nanosystems information storage and processing systems, 25 (2019) 3571-3580.
[36] S. Saranya, Q,M. Al-Mdallal, S. Javed, Shifted legendre collocation method for the solution of unsteady viscous-Ohmic dissipative hybrid ferrofluid flow over a cylinder. Nanomaterials 11 (2021) 1512.
[37] Q.M. Al-Mdallal, N. Indumathi, B. Ganga, A.K. Abdul Hakeem, Marangoni radiative effects of hybrid-nanofluids flow past a permeable surface with inclined magnetic field. Case Studies, Therm. Eng. 17 (2019) 100571.
[38] A. Renuka, M. Muthtamilselvan, Q.M. Al-Mdallal, D.H. Doh, B. Abdalla. Unsteaddy separted stagnation point flow of nanofluid past a moving flat surface in the presence of Buongiorno's model. J. Appl. Computational Mech. 2021 (online); DOI: 10.22055/JACM.2020.
[39] F.A. Soomro, R. Ul Haq, Q.M. Al-Mdallal, Q. Zhang, Heat generation/absorption and nonlinear radiation effects on stagnation point flow of nanofluid along a moving surface. Results, Physics 8 (2018) 404–414.
[40] R. Ul Haq, I. Rashid, Z.H. Khan, Q. Al-Mdallal, Flow of water based alumina and copper nanoparticles along a moving surface with variable temperature, J. Molecular Liquids 246 (2017) 354–362.
[41] Q.M. Al-Mdallal, A. Renuka, M. Muthtamilselvan, B. Din Abdalla, Ree-Eyring fluid flow of Cu-water nanofluid between infinite spinning disks with an effect of thermal radiation. Ain Shams Engineering Journal, Online (2021).
[42] A. Ziyad, A. Alhussain, M. Renuka, M. Muthtamilselvan, A magneto-bioconvective and thermal conductivity enhancement in nanofluid flow containing gyrotactic microorganism. Case Studies, Therm. Eng. 23 (2021), paper number 100809.
[43] N.S. Wahid, N.M. Arifin, N.S. Khashi'ie, I. Pop, Hybrid Nanofluid Slip Flow over an Exponentially Stretching/Shrinking Permeable Sheet with Heat Generation, Mathematics 9 (1) (2021) 30.
[44] E.H. Aly, M. Benlahsen, M. Guedda, Similarity solutions of a MHD boundary-layer flow past a continuous moving surface, Int. J. Eng. Sci. 45 (2–8) (2007) 486–503.
[45] H.F. Oztop, E. Abu-Nada, Numerical study of natural convection in partially heated rectangular enclosures filled with nanofluids, Int. J. Heat Fluid Flow 29 (5) (2008) 1326–1336.
[46] P.D. Weidman, D.G. Kubitschek, A.M. Davis, The effect of transpiration on self-similar boundary layer flow over moving surfaces, Int. J. Eng. Sci. 44 (11–12) (2006) 730–737.
[47] J.H. Merkin, On dual solutions occurring in mixed convection in a porous medium, J. Eng. Math. 20 (1985) 171–179.
[48] S.D. Harris, D.B. Ingham, I. Pop, Mixed convection boundary layer flow near the stagnation point on a vertical surface in a porous medium: Brinkman model with slip, Transp. Porous Media 77 (2) (2009) 267–285.
[49] A.M. Rohni, S. Ahmad, I. Pop, Boundary layer flow over a moving surface in a nanofluid beneath a uniform free stream, Int. J. Numer. Methods Heat Fluid Flow 21 (7) (2011) 828–846.